Supporting Information for

Rapid Secondary Organic Aerosol Formation at the Air–Water Interface from Methoxyphenols in Wildfire Emissions: UVA-Driven S(IV) Photooxidation to Organosulfates

Baohua Cai,[1] Yuanlong Huang,[2] Wenqing Jiang,[3] Yanchen Li,[1] Yali Li,[1] Jinghao Zhai,[1,4] Yaling Zeng,[1,4] Jianhuai Ye,[1,4] Huizhong Shen,[1,4] Chen Wang,[1,4] Lei Zhu,[1,4] Tzung-May Fu,[1,4] Qi Zhang,[3]* Xin Yang[1,4]*

*Qi Zhang and Xin Yang.

Email: yangx@sustech.edu.cn and dkwzhang@ucdavis.edu

This PDF file includes:

Supporting text
Figures S1 to S29
Table S1
SI References

Supplementary Text

Distribution factor of GUA and aqueous phase calculation (X_{aq})

The concentrations of phenolic compounds in the gas and aqueous phases were calculated as a function of liquid water content at 5 ºC. Henry's law constant for guaiacol (GUA) at 278 k ($K_{H,278K}$) were calculated from the measured value at 289 K using the enthalpy of dissolution (ΔH_{sol}) [1]:

$$K_{H,278K} = K_{H,298K} \times \exp\left(\frac{\Delta H_{sol}}{R} \times \left(\frac{1}{298K} - \frac{1}{278K}\right)\right)$$

where R is the ideal-gas constant (8.314 J K^{-1} mol^{-1}). $K_{H,298K}$ is 870 M atm^{-1}. So that the $K_{H,278K}$ is 5326 M atm^{-1}.

The distribution factor ($f_{phenols}$) and the aqueous-phase fraction (X_{aq}) were then calculated using [2]:

$$f_{phenols} = 10^{-6} K_{H,279K} RTL$$

$$X_{aq} = \frac{f_{phenols}}{1 + f_{phenols}}$$

where R = 0.08205 atm L mol^{-1} K^{-1}; T = 278 K. L is the liquid water content in cloud or fog, expressed in g m^{-3}.

Relative rate technique [3]

Experimental Methods

All experiments were performed in a 25 mL airtight Pyrex tube with a magnetic stirrer and a bubble tube for feeding high-purity zero air or nitrogen under 370 nm light. A 20 mL reaction solution of the GUA and phenol, and Na_2SO_3 or $Na_2S_2O_8$. The pH of the reaction solution is regulated by H_2SO_4 and NaOH. The pH of solutions was measured with a pH meter REDOX potentiometer Conductivity meter (AZ-86555) that was calibrated with commercial pH standards. Aliquots of 3 mL reaction solution, to which 0.30 mL MeOH was added to stop the reaction, were sampled for chemical analysis every 15 min for 1h. Each experiment was repeated at least twice.

Model 1 experimental conditions: [guaiacol] = 0.1 mM, [phenol] = 0.1 mM, [Na_2SO_3] = 3.0 mM, with zero air bubbling, 370 nm light irradiation, room temperature.
Model 2 experimental conditions: [guaiacol] = 0.1 mM, [phenol] = 0.1 mM, [$Na_2S_2O_8$] = 3.0 mM, with zero air bubbling, 370 nm light irradiation, room temperature.

$$S_2O_8^{2-} + UVA \rightarrow 2SO_4^{\bullet -}$$

The rate constant calculation

Photodegradation correction is based on pseudo-first-order kinetics, where k is the second-order rate constant for reactions of phenol (PhOH) and guaiacol (GUA) with $SO_4^{\cdot -}$. The effective pseudo-first-order rate constants is $k' = k[SO_4^{\cdot -}]_{ss}$. and J = 0.0016 min^{-1} is the first order photolytic rate coefficient for GUA in the photodegradation control experiments (Phenol is basically non-photodegradation at 370 nm irradiation).

$$[GUA]_t = [GUA]_0 \exp\left(-(k'_{GUA} + J) \times t\right)$$
$$[PhOH]_t = [PhOH]_0 \exp\left(-k'_{phOH} \times t\right)$$

Therefore

$$\ln\frac{[GUA]_0}{[GUA]_t} = (k'_{GUA} + J) \times t$$

$$\ln\frac{[PhOH]_0}{[PhOH]_t} = k'_{phOH} \times t$$

A ratio of k_{GUA}/k_{phOH} is achieved by:

$$\frac{k_{GUA}}{k_{phOH}} = \frac{k'_{GUA} + J}{k'_{phOH}} = \frac{\ln\frac{[GUA]_0}{[GUA]_t} - J \times t}{\ln\frac{[PhOH]_0}{[PhOH]_t}}$$

Coordinates of the structure

SO_3^{2-}:

S 0.00015600 0.00018800 0.36151200
O 1.38572000 -0.24335000 -0.24107700
O -0.48223400 1.32083300 -0.24107800
O -0.90379800 -1.07785700 -0.24086900

Sum of electronic energy and thermal correction to G: -623.4450423 a.u.

O_2:

O 0.00000000 0.00000000 0.59360300
O 0.00000000 0.00000000 -0.59360300

Sum of electronic energy and thermal correction to G: -150.1566305 a.u.

[SO_3^{2-} + O_2]:

S 0.96864400 -0.04418400 -0.20653100
O 2.38919700 -0.44069500 -0.61297600
O 1.06524600 1.41394400 0.24872600
O 0.66735600 -0.84784400 1.05959300
O -2.94989700 0.52084100 0.09346400
O -3.10919000 -0.55787800 -0.37574400

Sum of electronic energy and thermal correction to G: -773.5908018 a.u.

$SO_3^{\cdot-}$:

S 0.00001100 -0.00005500 0.23076000
O 1.26234500 -0.64995800 -0.15385200
O -0.06818600 1.41809700 -0.15382000
O -1.19418100 -0.76802900 -0.15384700

Sum of electronic energy and thermal correction to G: -623.2845358 a.u.

$O_2^{\cdot-}$:

O 0.00000000 0.00000000 0.65791100
O 0.00000000 0.00000000 -0.65791100

Sum of electronic energy and thermal correction to G: -150.2964283 a.u.

$SO_5^{\cdot-}$:

S 0.45122400 0.14219000 0.00000000
O 0.73865300 1.54990000 0.00000000
O 0.73865300 -0.56776700 1.21625700
O 0.73865300 -0.56776700 -1.21625700
O -1.28477600 0.23510800 0.00000000
O -1.83363100 -0.93385400 0.00000000

Sum of electronic energy and thermal correction to G: -773.4558495 a.u.

Fig. S1. The glass instrument was used in the experiment.

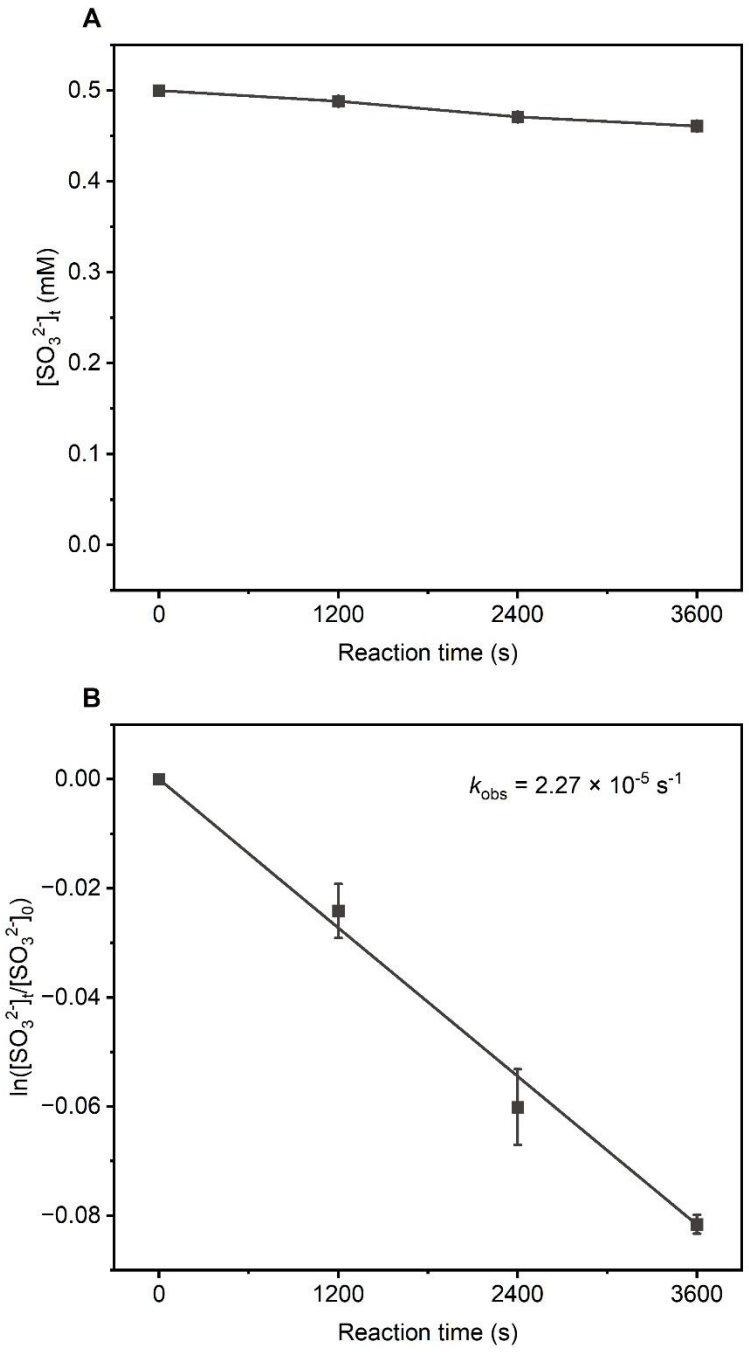

Fig. S2. (A) Kinetics of the aqueous-phase oxidation of SO_3^{2-} under dark conditions. (B) The pseudo-first-order rate constant for the oxidation of Na_2SO_3. Error bars represent the standard deviation from at least two independent experiments. Experimental conditions: [Na_2SO_3] = 0.5 mM, pH = 4.0 ± 0.1, zero-air bubbling, room temperature, Solution acidity was controlled using a phosphoric acid / phosphate buffer system.

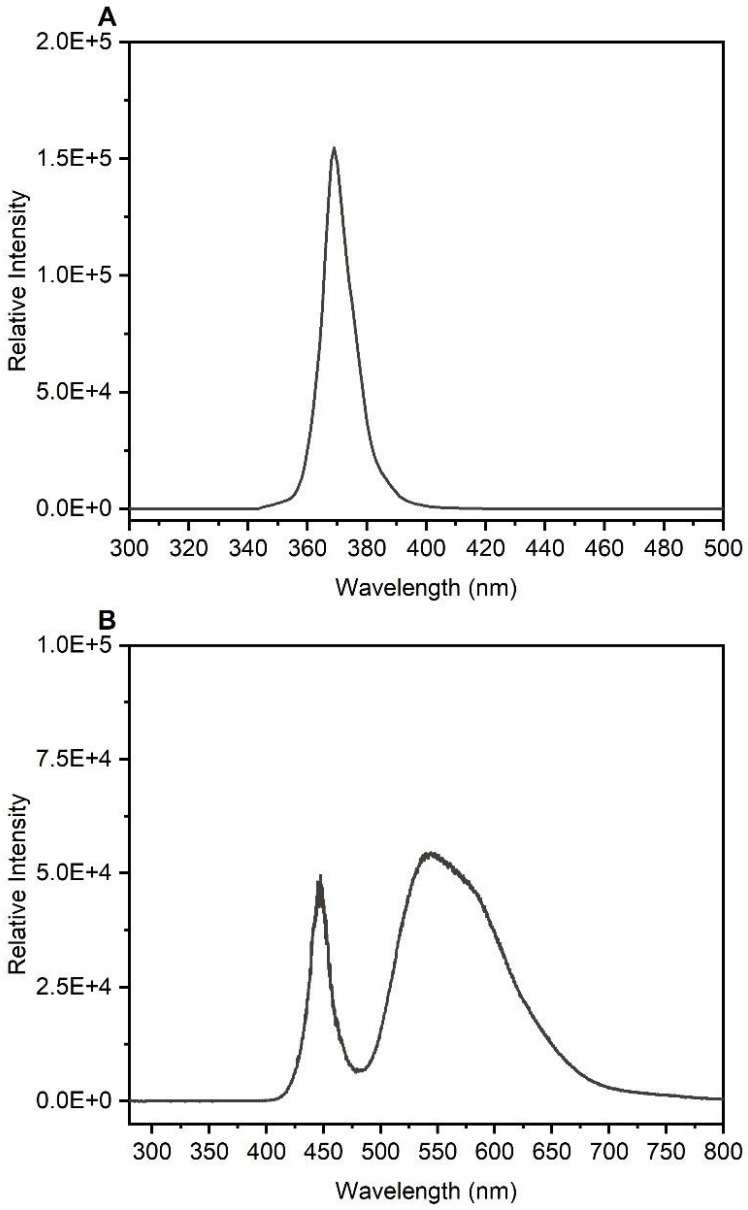

Fig. S3. (A) The Kessil PR160L-370nm lamp spectra. (B) The LED lamp spectra (Beijing Perfectlight Technology Co., Ltd.).

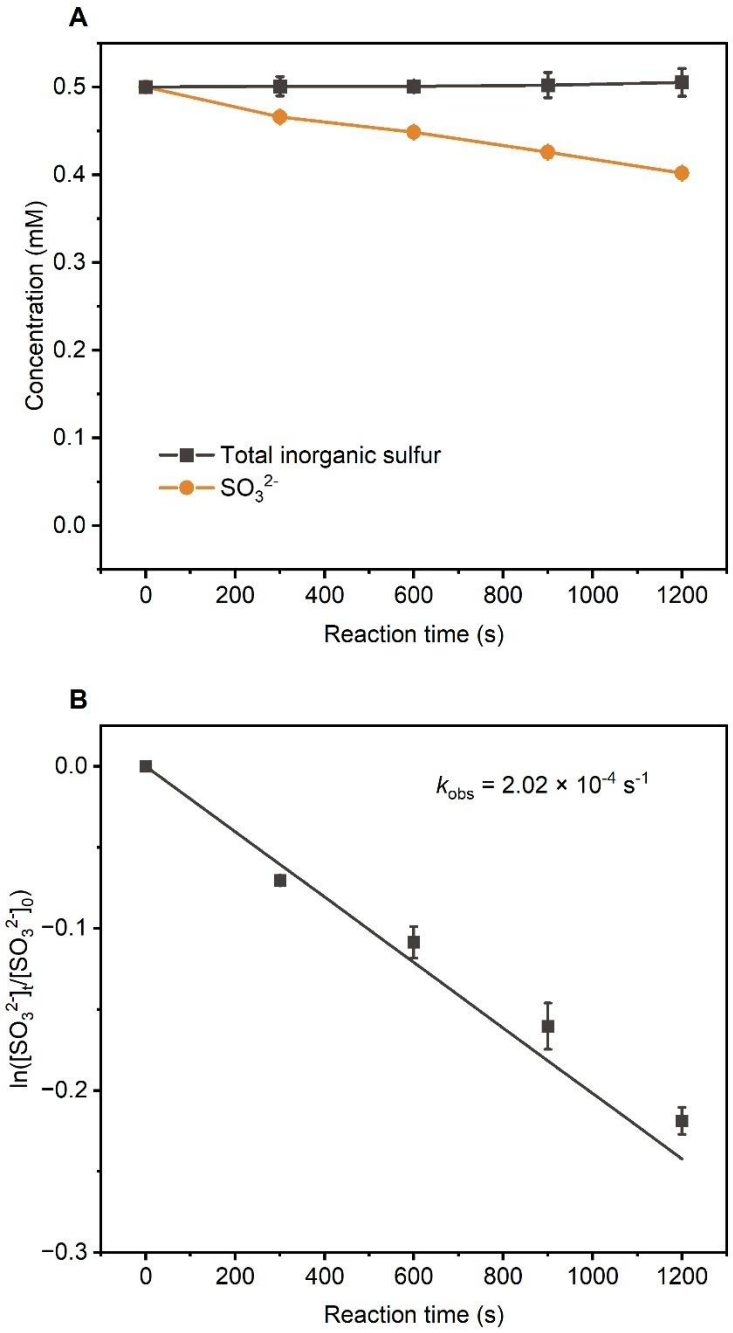

Fig. S4. (A) Kinetics of the aqueous-phase oxidation of SO_3^{2-} under 370 nm irradiation. (B) The pseudo-first-order rate constant for the photooxidation of Na_2SO_3. Error bars represent the standard deviation from at least two independent experiments. Experimental conditions: [Na_2SO_3] = 0.5 mM, pH = 4.0 ± 0.1, zero-air bubbling, 370 nm light irradiation, room temperature. Solution acidity was controlled using a phosphoric acid / phosphate buffer system.

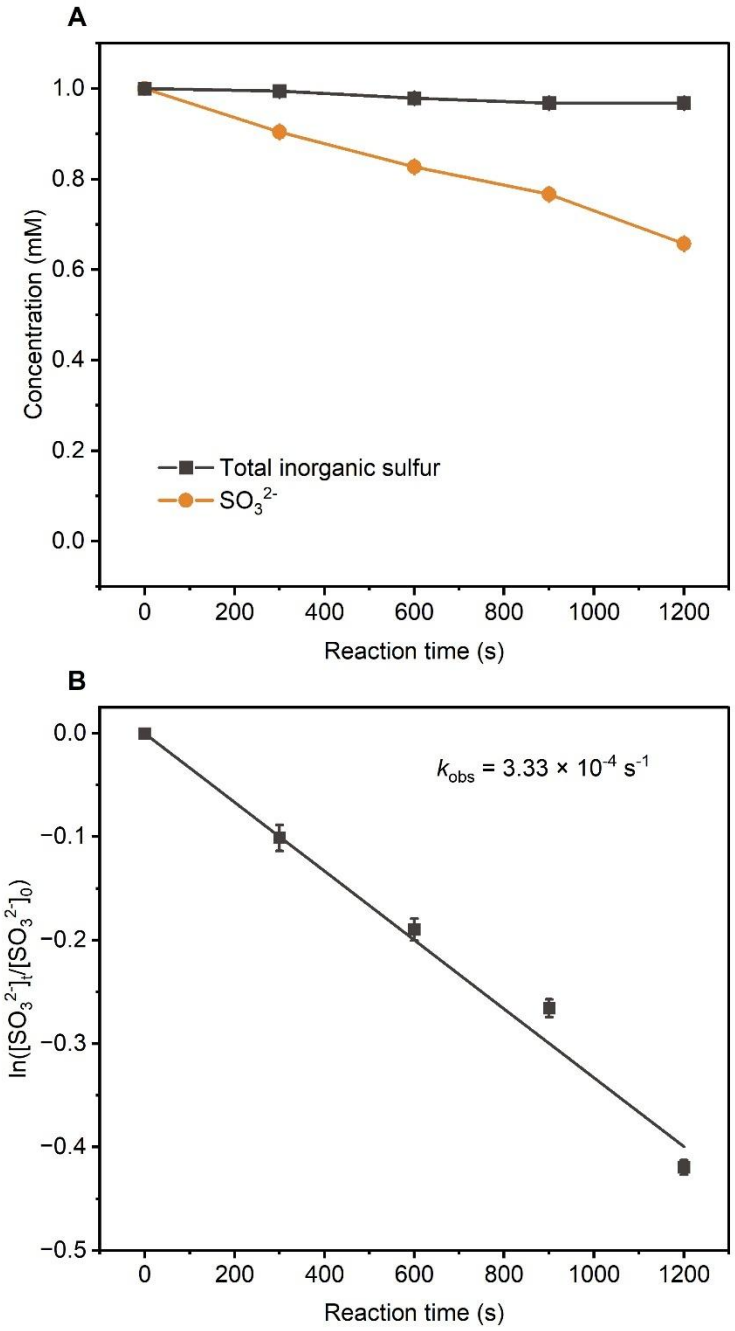

Fig. S5. (A) Kinetics of the aqueous-phase oxidation of SO_3^{2-} under 370 nm irradiation. (B) The pseudo-first-order rate constant for the photooxidation of Na_2SO_3. Error bars represent the standard deviation from at least two independent experiments. Experimental conditions: [Na_2SO_3] = 1.0 mM, pH = 4.0 ± 0.1, zero-air bubbling, 370 nm light irradiation, room temperature. Solution acidity was controlled using a phosphoric acid / phosphate buffer system.

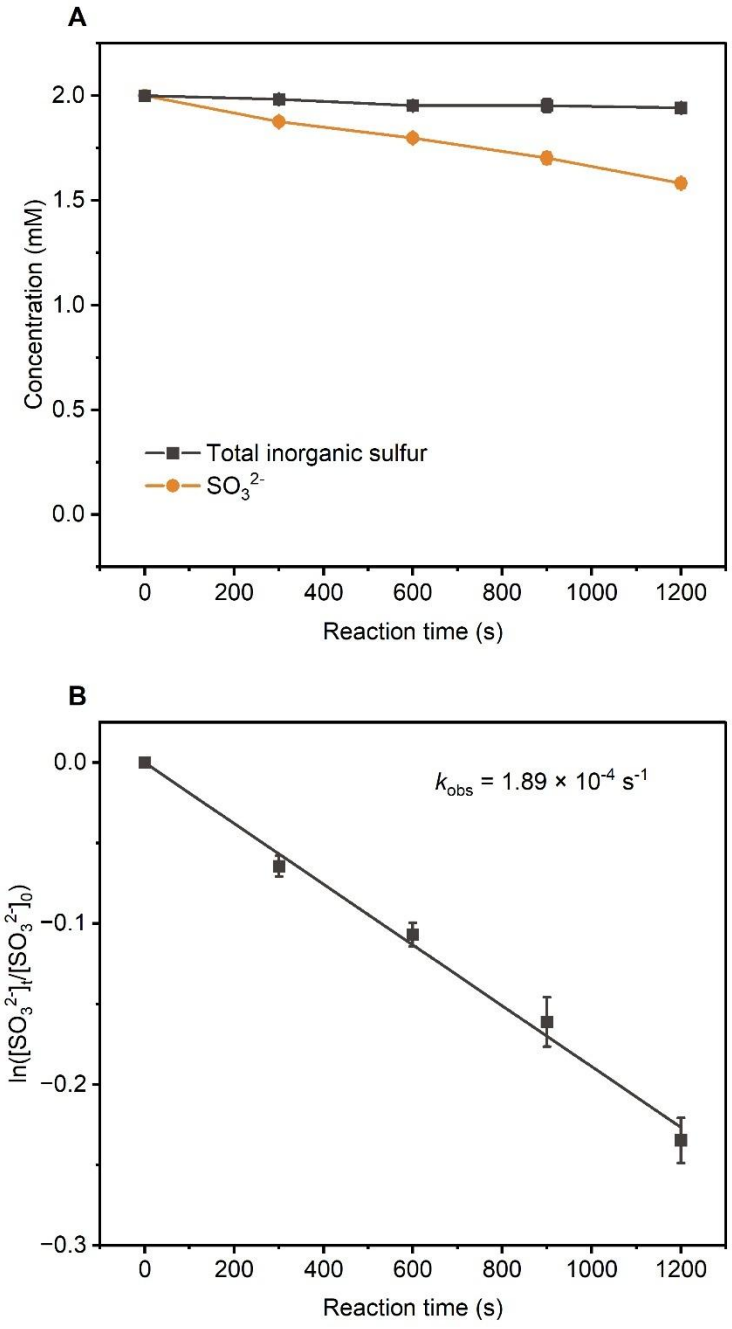

Fig. S6. (A) Kinetics of the aqueous-phase oxidation of SO_3^{2-} under 370 nm irradiation. (B) The pseudo-first-order rate constant for the photooxidation of Na_2SO_3. Error bars represent the standard deviation from at least two independent experiments. Experimental conditions: [Na_2SO_3] = 2.0 mM, pH = 4.0 ± 0.1, zero-air bubbling, 370 nm light irradiation, room temperature. Solution acidity was controlled using a phosphoric acid / phosphate buffer system.

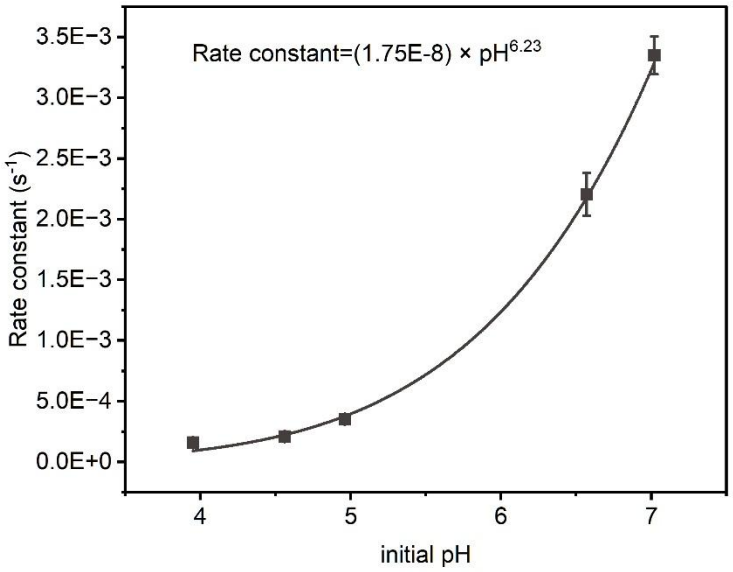

Fig. S7. Variation in the oxidation rate constants for SO_3^{2-} under 370 nm light as a function of initial pH. Error bars represent the standard deviation from at least two independent experiments. Experimental conditions: $[Na_2SO_3]$ = 0.5 mM, zero-air bubbling, 370 nm light, room temperature. Solution acidity was controlled using a phosphoric acid / phosphate buffer system.

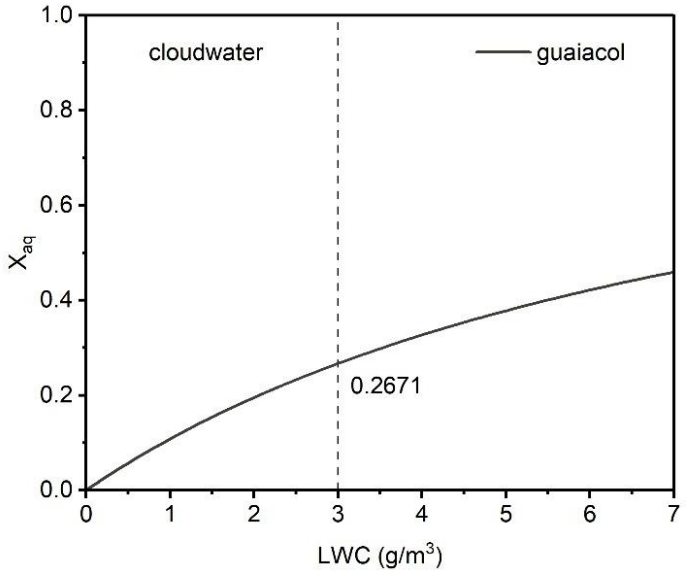

Fig. S8. The gas-water distribution of GUA under an air temperature of 5 °C and varying liquid water content.

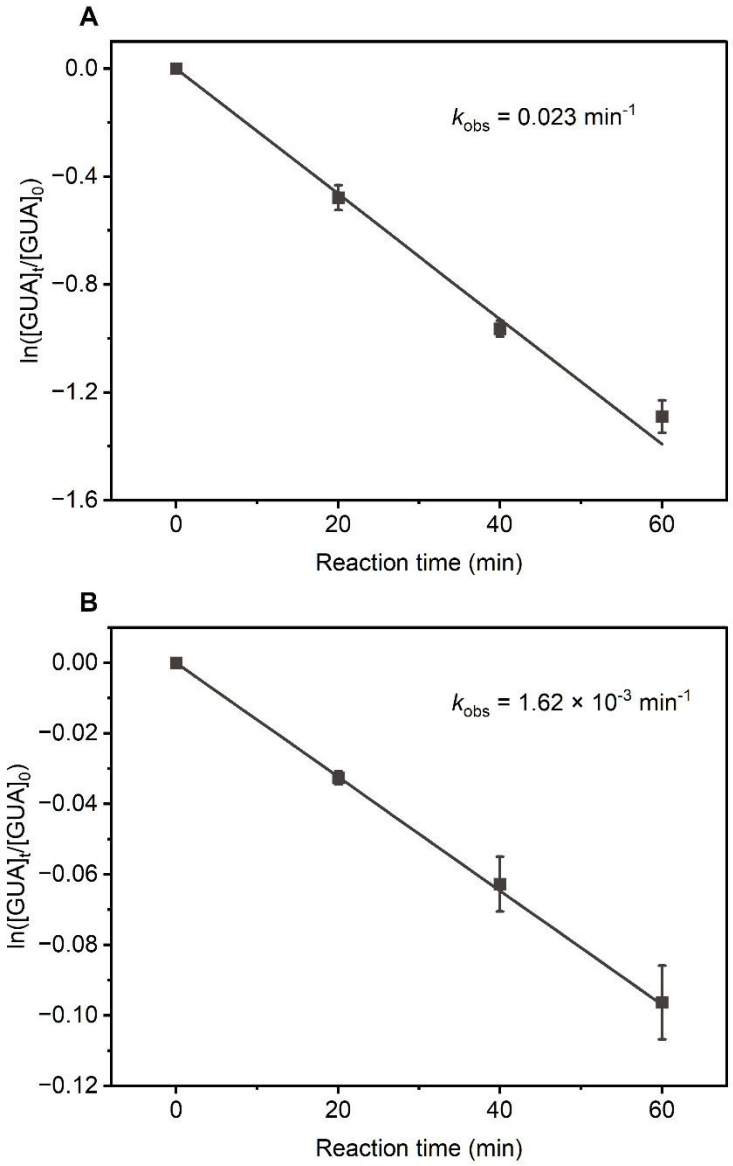

Fig. S9. (A) The pseudo-first-order rate constant for the reaction between GUA and Na_2SO_3 under 370 nm irradiation. (B) The pseudo-first-order rate constant for the photooxidation of GUA under 370 nm irradiation. Error bars represent the standard deviation from at least two independent experiments. Experimental conditions: [guaiacol] = 0.1 mM, [Na_2SO_3] = 2.0 mM, pH = 4.0 ± 0.1, with zero-air bubbling, 370 nm light irradiation, room temperature.

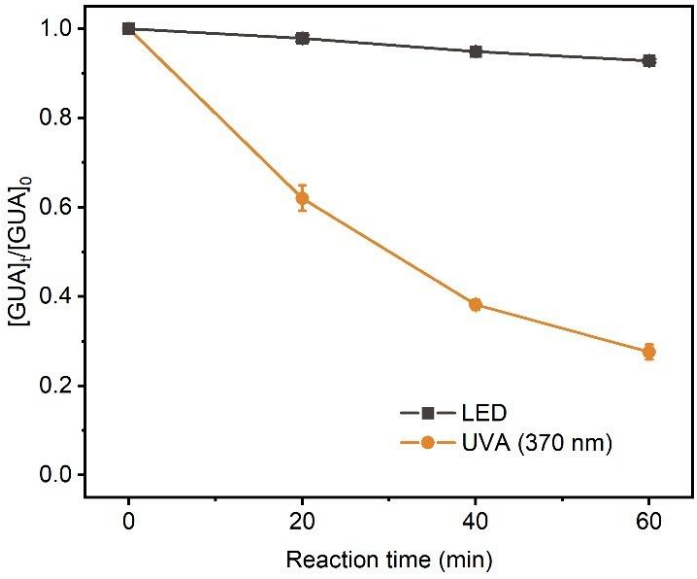

Fig. S10. Effects of different light sources on the reaction. Error bars represent the standard deviation from at least two independent experiments. Experimental conditions: [guaiacol] = 0.1 mM, [Na_2SO_3] = 2 mM, pH = 4.0 ± 0.1, with zero-air bubbling, 370 nm light and LED irradiation, room temperature.

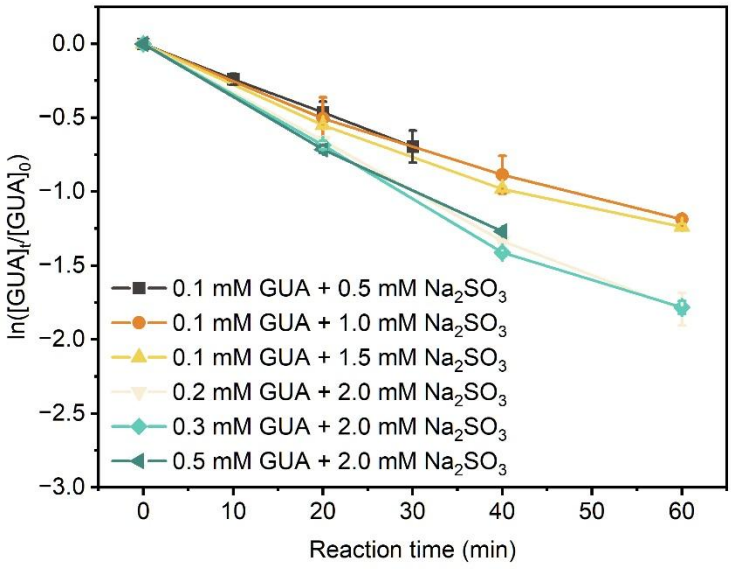

Fig. S11. Reaction kinetics of guaiacol degradation in aqueous solution as a function of Na_2SO_3 concentration. Error bars represent the standard deviation from at least two independent experiments. Experimental conditions: [guaiacol] = 0.1 mM, pH = 4.0 ± 0.1, zero-air bubbling, 370 nm irradiation, room temperature.

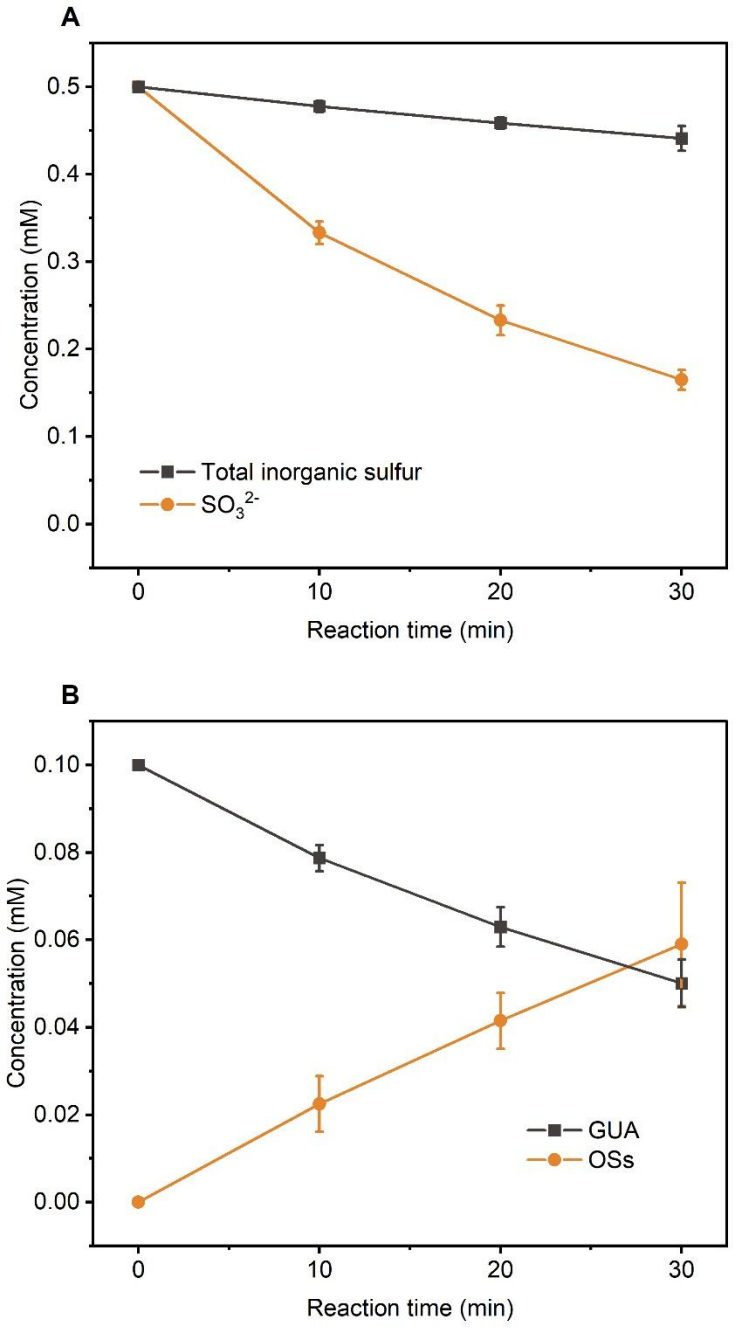

Fig. S12. Kinetics of the aqueous-phase reaction between guaiacol and Na_2SO_3 under 370 nm irradiation. (A) Time evolution of SO_3^{2-} and total inorganic sulfur. (B) Concentrations of guaiacol and estimated organosulfates (OSs) over time. [OSs] = 0.5 mM – [total inorganic sulfur], where 0.5 mM is the initial concentration of SO_3^{2-}. Error bars represent the standard deviation from at least two independent experiments. Experimental conditions: [guaiacol] = 0.1 mM, $[Na_2SO_3]_0$ = 0.5 mM, pH = 4.0 ± 0.1, zero-air bubbling, 370 nm light irradiation, room temperature. Solution acidity was controlled using a phosphoric acid / phosphate buffer system.

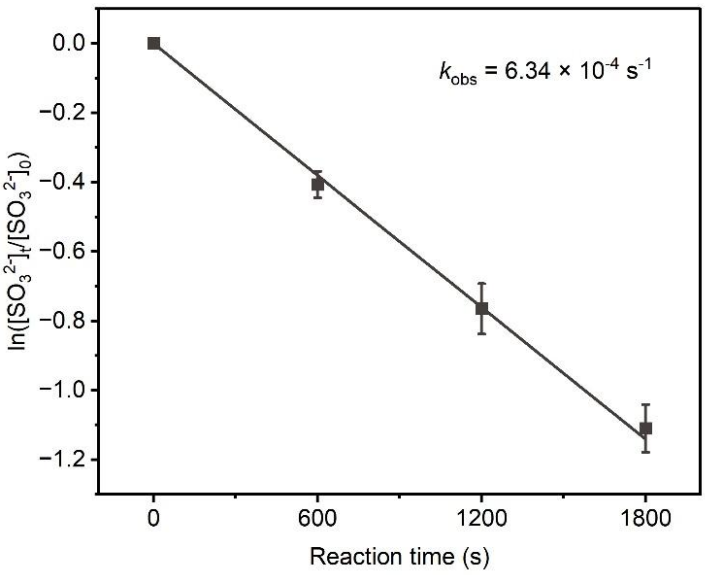

Fig. S13. Pseudo-first-order rate constant for the photooxidation of Na_2SO_3 in the presence of GUA. Error bars represent the standard deviation from at least two independent experiments. Experimental conditions: [GUA] = 0.1 mM, [Na_2SO_3] = 0.5 mM, pH = 4.0 ± 0.1, zero-air bubbling, 370 nm irradiation, room temperature. Solution acidity was controlled using a phosphoric acid / phosphate buffer system.

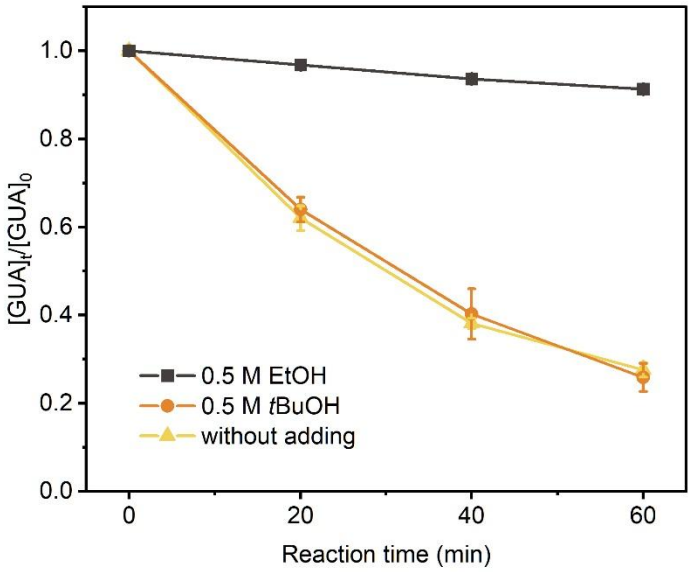

Fig. S14. Kinetics of the aqueous-phase reaction between guaiacol and Na_2SO_3 under 370 nm irradiation in the presence of different radical quenchers. Error bars represent the standard deviation from at least two independent experiments. Experimental conditions: [guaiacol] = 0.1 mM, [Na_2SO_3] = 2.0 mM, [EtOH] = 0.5 M, [*t*BuOH] = 0.5 M, pH = 4.0 ± 0.1, zero-air bubbling, 370 nm irradiation, room temperature.

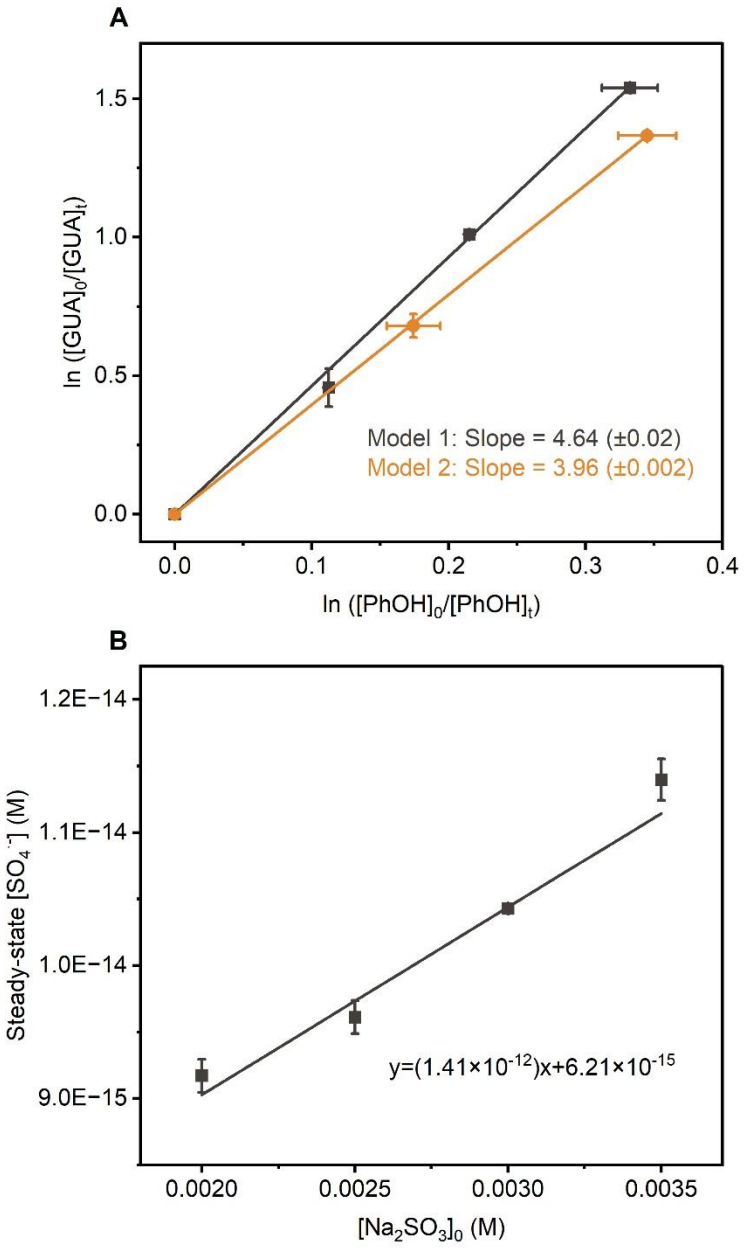

Fig. S15. (A) Relative rate determination of GUA vs. phenol (PhOH) under two conditions: Model 1 – 0.1 mM GUA, 0.1 mM PhOH, and 3.0 mM Na_2SO_3; Model 2 – 0.1 mM GUA, 0.1 mM PhOH, and 3.0 mM $Na_2S_2O_8$. (B) Steady-state concentration of $SO_4^{\bullet-}$ as a function of Na_2SO_3 concentration. Error bars represent the standard deviation from at least two independent experiments. Experimental conditions: zero-air bubbling, 370 nm irradiation, room temperature.

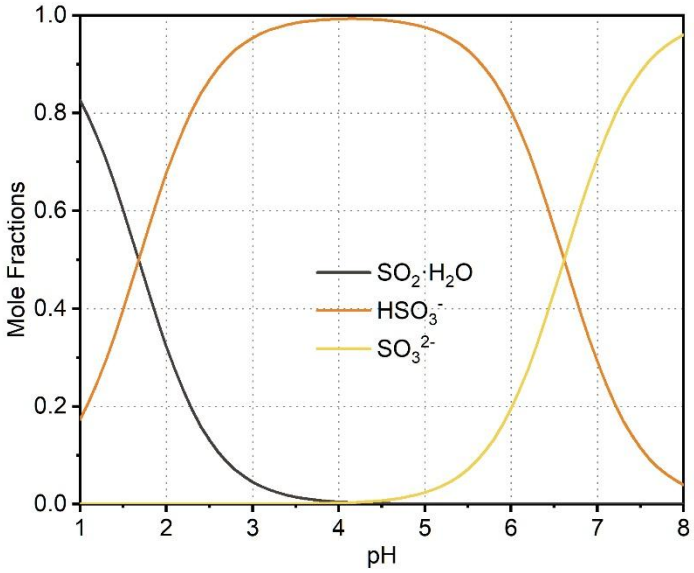

Fig. S16. Speciation of S(IV) inorganic compounds based on their pKa values.

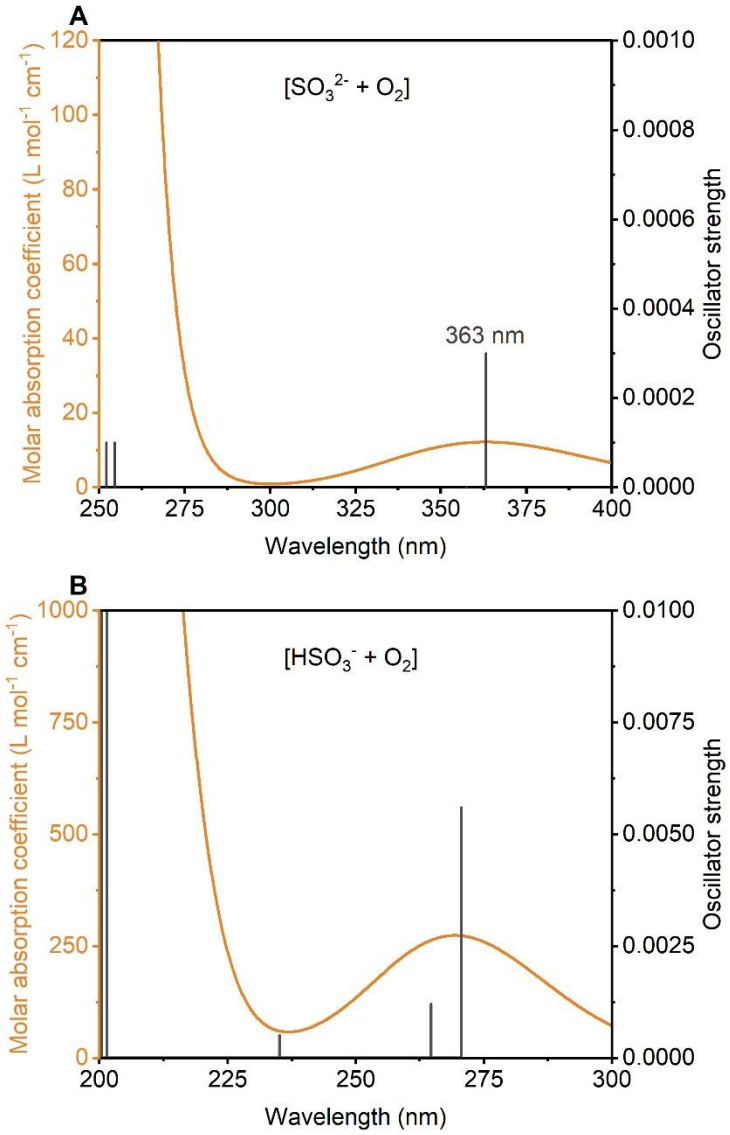

Fig. S17. Vertical excitation spectra. A [SO_3^{2-} + O_2] complex and B [HSO_3^- + O_2] complex, calculated using TDDFT at the M06-2X/ma-TZVP/SMD(water) level.

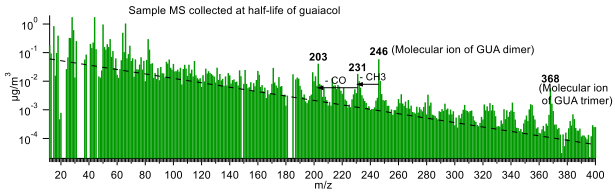

Fig. S18. High-resolution aerosol mass spectrum (HR-ToF-AMS) of low-volatility organics in the sample solution following 50% guaiacol depletion, obtained from the experiment with 0.5 mM guaiacol, 0.5 mM Na_2SO_3, 0.48 mM H_2SO_4. Peaks corresponding to the GUA dimer, its fragment ions, and trimer ions are indicated. The broken line is added to guide the eye

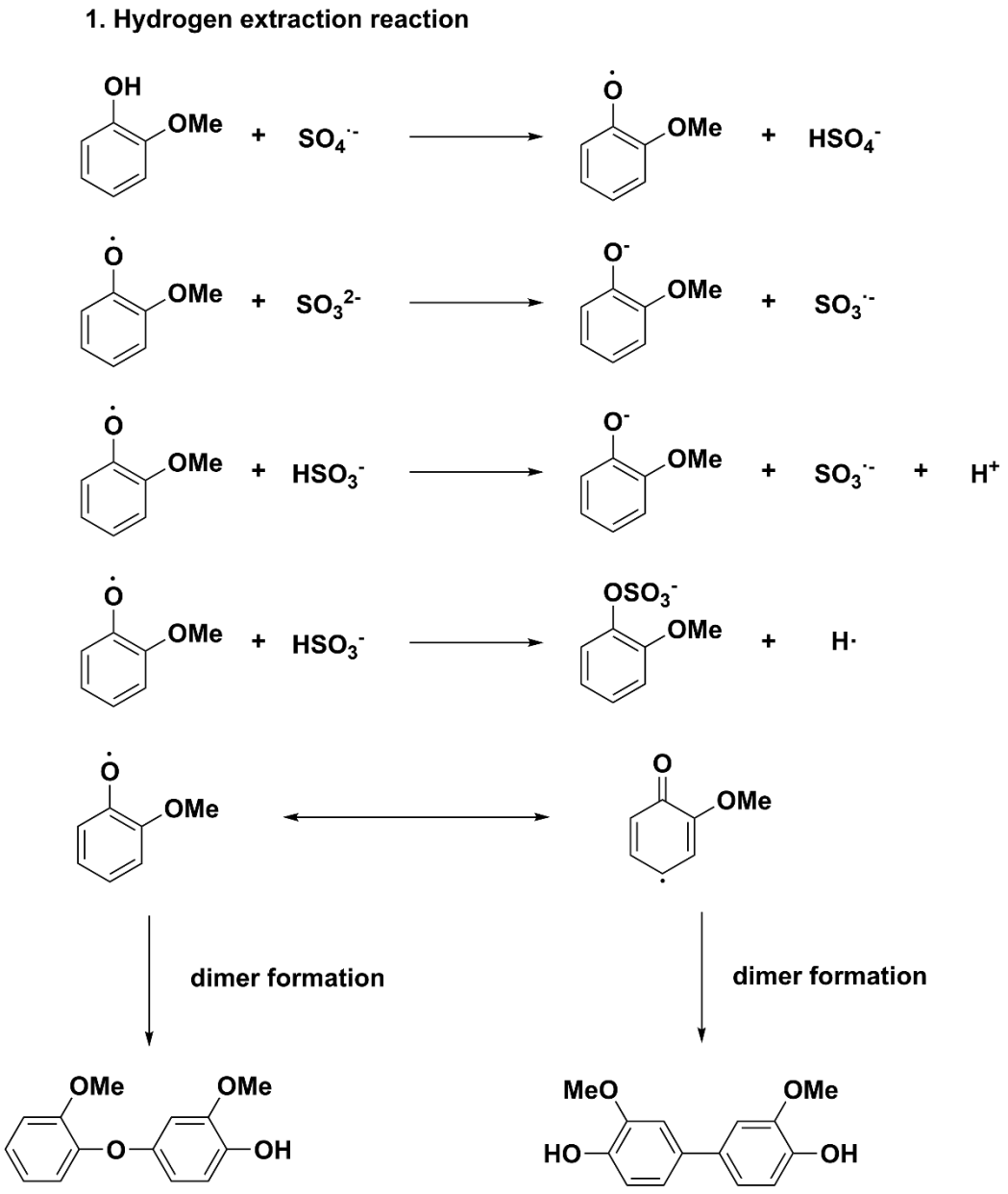

Fig. S19. The possible reaction mechanism between GUA and $SO_4^{\bullet-}$.

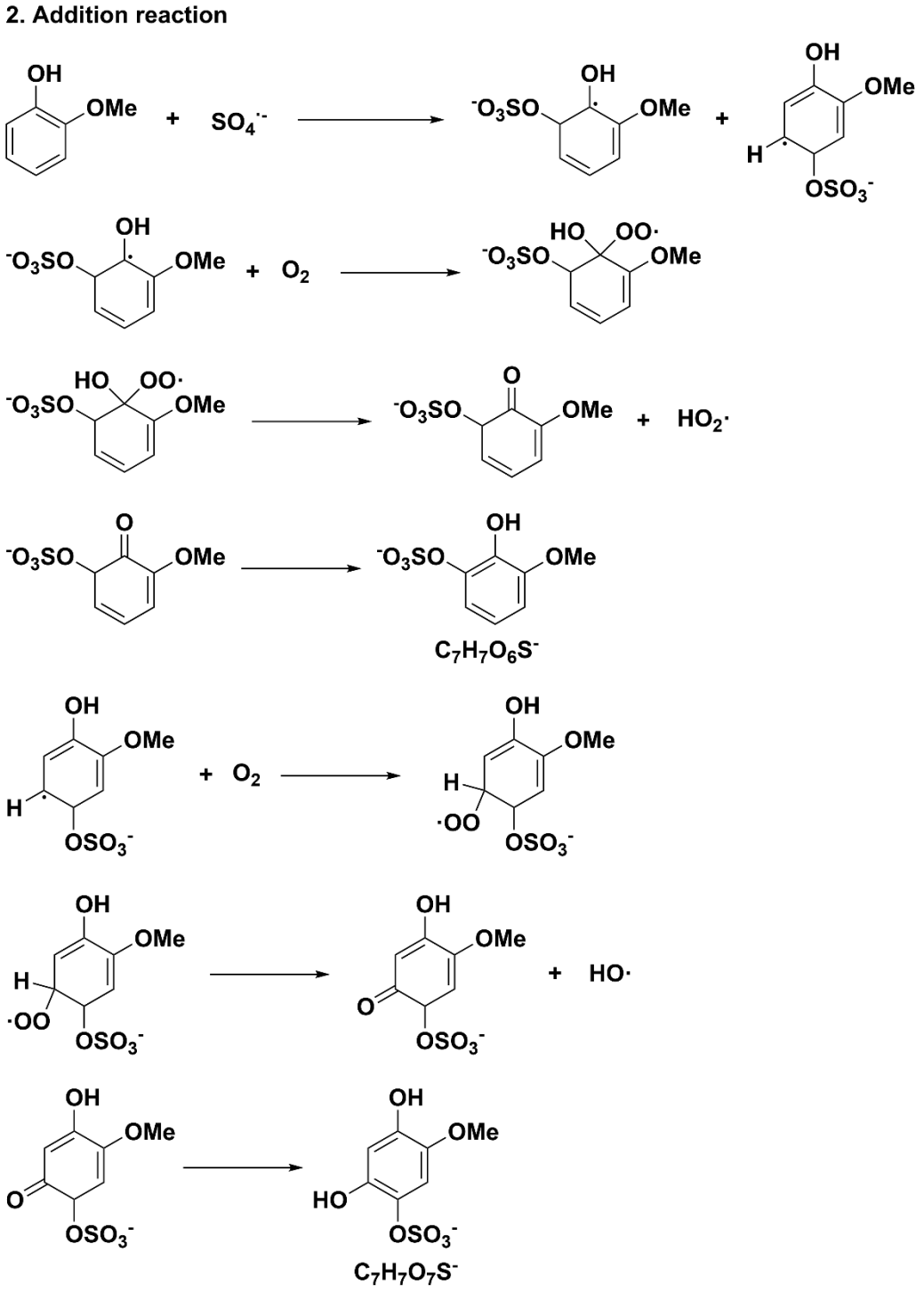

Fig. S20. The possible reaction mechanism between GUA and $SO_4^{\bullet-}$.

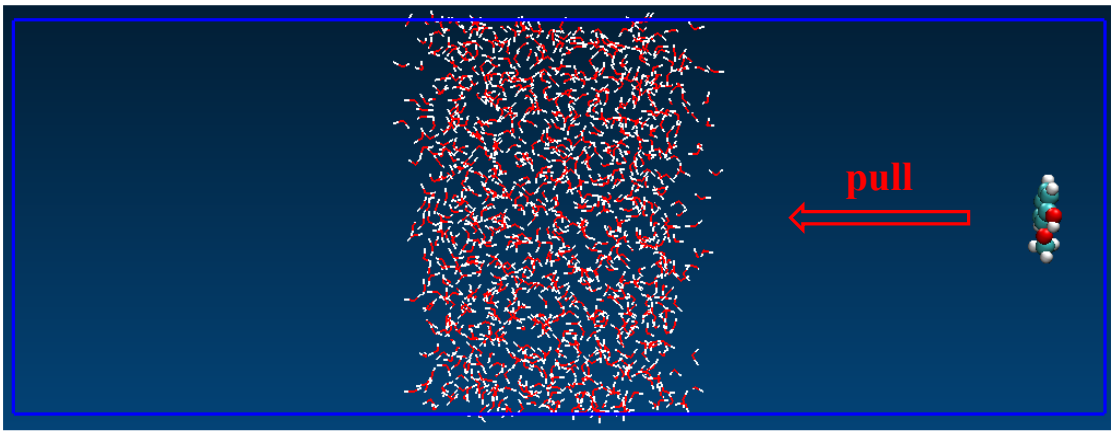

Fig. S21. Classical molecular dynamics simulation uses the Weighted Histogram Analysis Method (WHAM) to calculate the potential of mean force (PMF). GUA was positioned at coordinates (1.8, 1.8, 9.5 nm), while water clusters were centered in the simulation box at (3.6, 3.6, 10 nm) with a thickness of 2.35 nm. The white, red and dark cyan balls symbolize H, O, and C atoms, respectively.

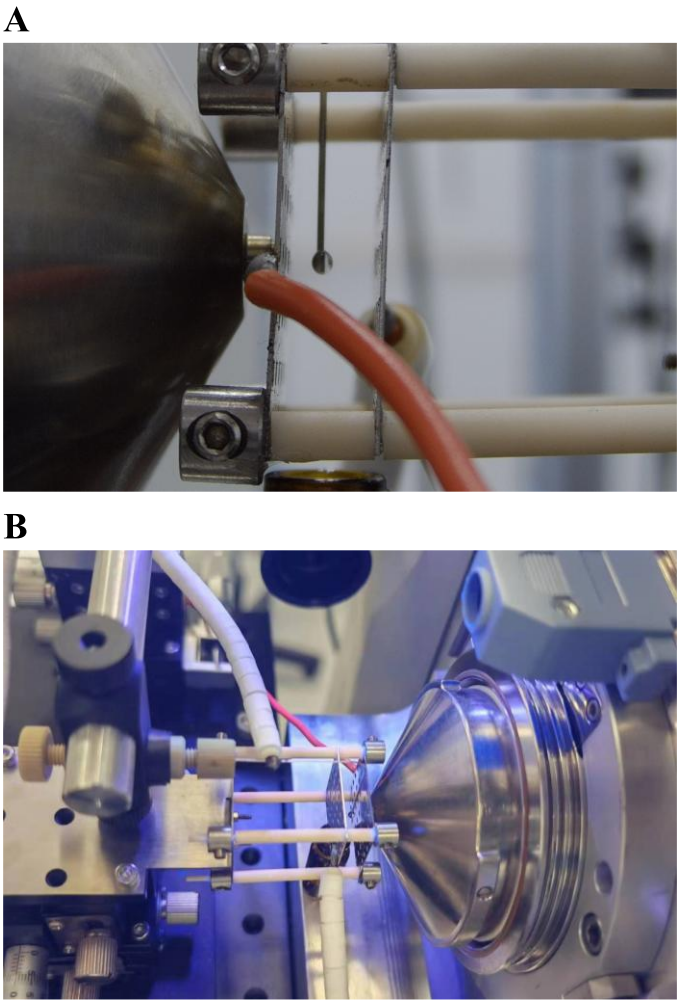

Fig. S22. FIDI-MS setup used to investigate the photodegradation of GUA and Na_2SO_3 under 370 nm irradiation.

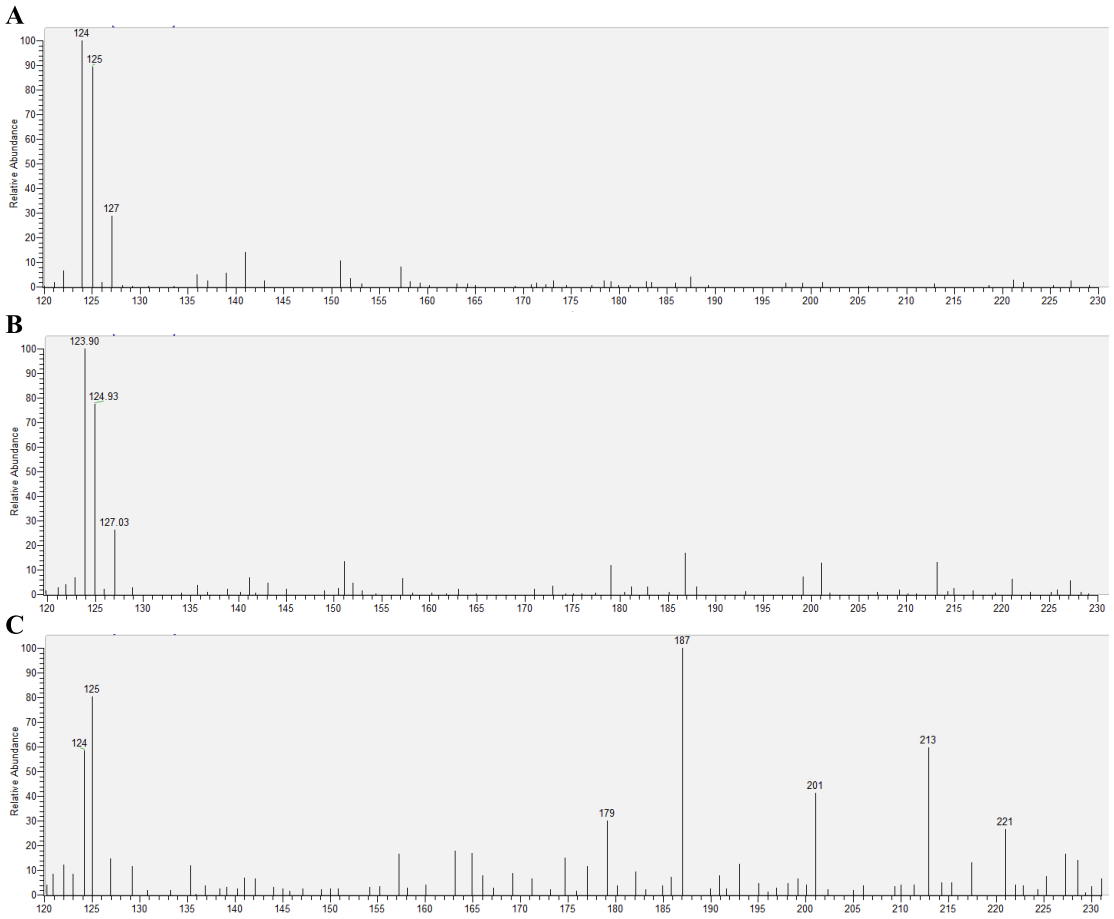

Fig. S23. FIDI-MS analysis of the photodegradation of GUA and Na_2SO_3 under 370 nm irradiation. (A) Mass spectrum of 0.1 mM GUA solution droplets after exposure to air for 2 minutes without irradiation. (B) Mass spectrum of 0.1 mM GUA solution droplets exposed to air for 1 minute followed by 1 minute for 370 nm irradiation. (C) Mass spectrum of 0.1 mM GUA and 3.0 mM Na_2SO_3 solution droplets exposed to air for 1 minute and then irradiated at 370 nm for 1 minute.

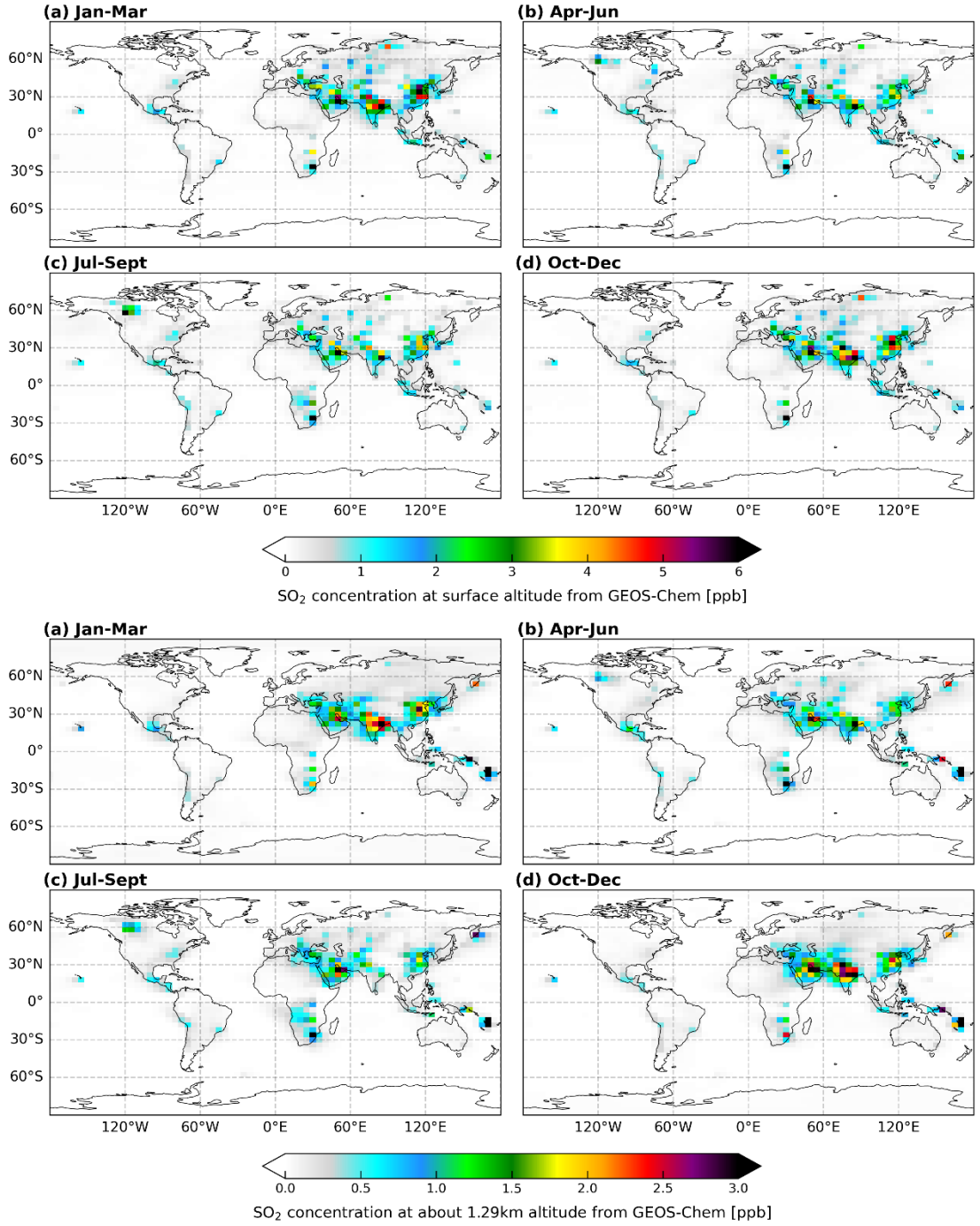

Fig. S24. Seasonal variations of global gas-phase SO_2 concentrations in 2023 from GEOS-Chem simulations. Top four panels: SO_2 concentrations at the surface level. Bottom four panels: SO_2 concentrations at 1.29 km altitude.

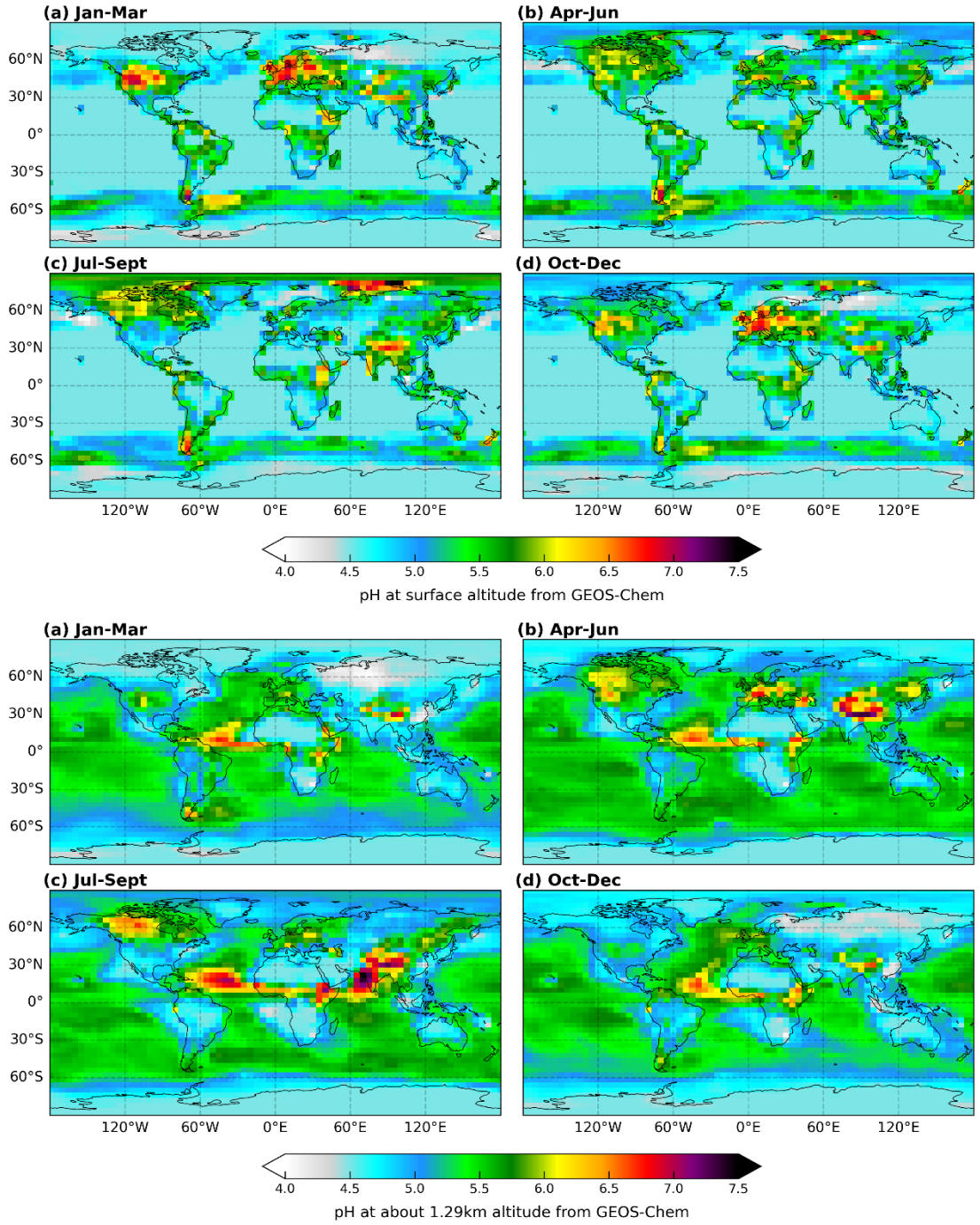

Fig. S25. The global cloud pH value in 2023 for different seasons at surface and 1.29 km altitude.

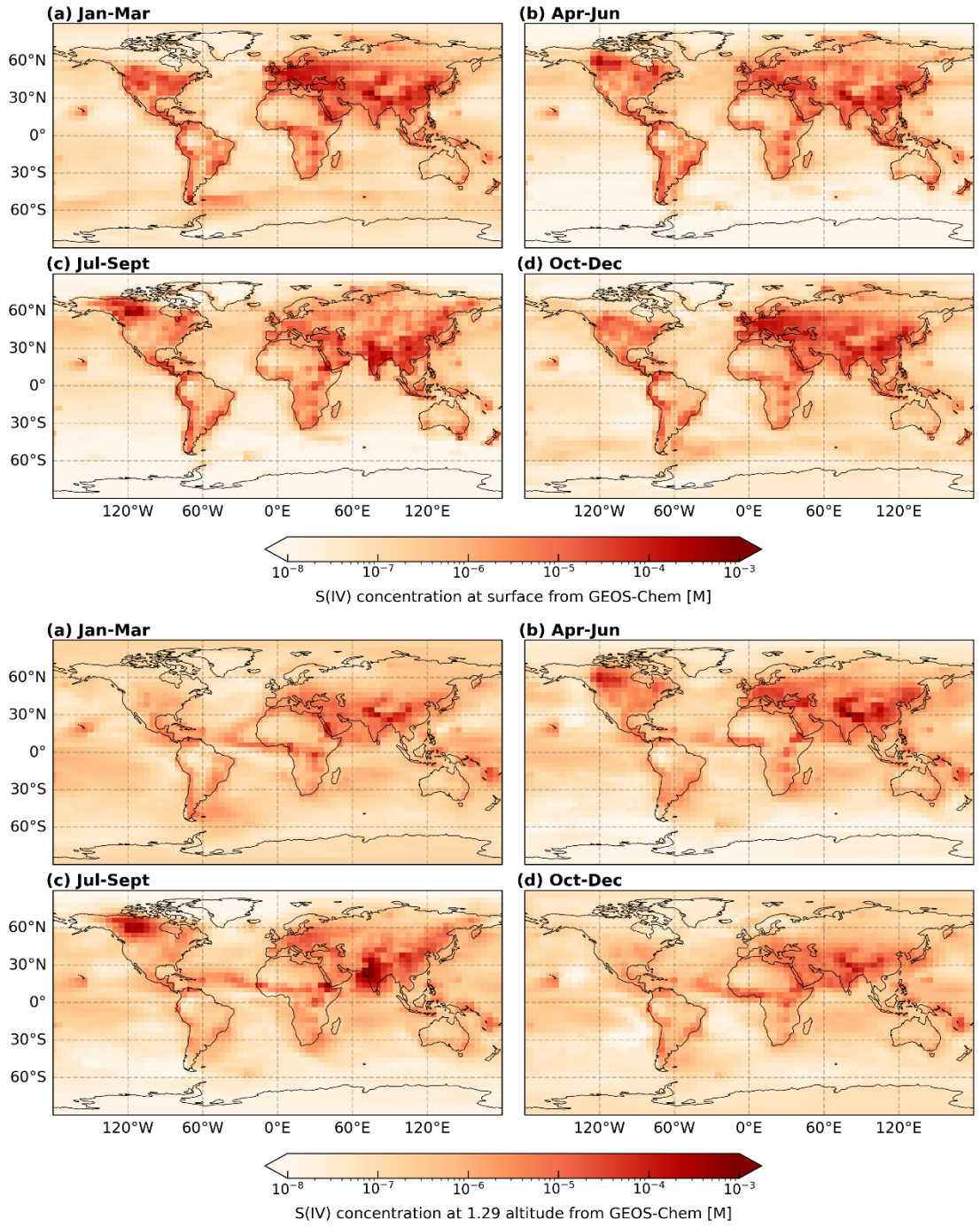

Fig. S26. The global aqueous-phase S(IV) concentration in 2023 for different seasons at surface and 1.29 km altitude.

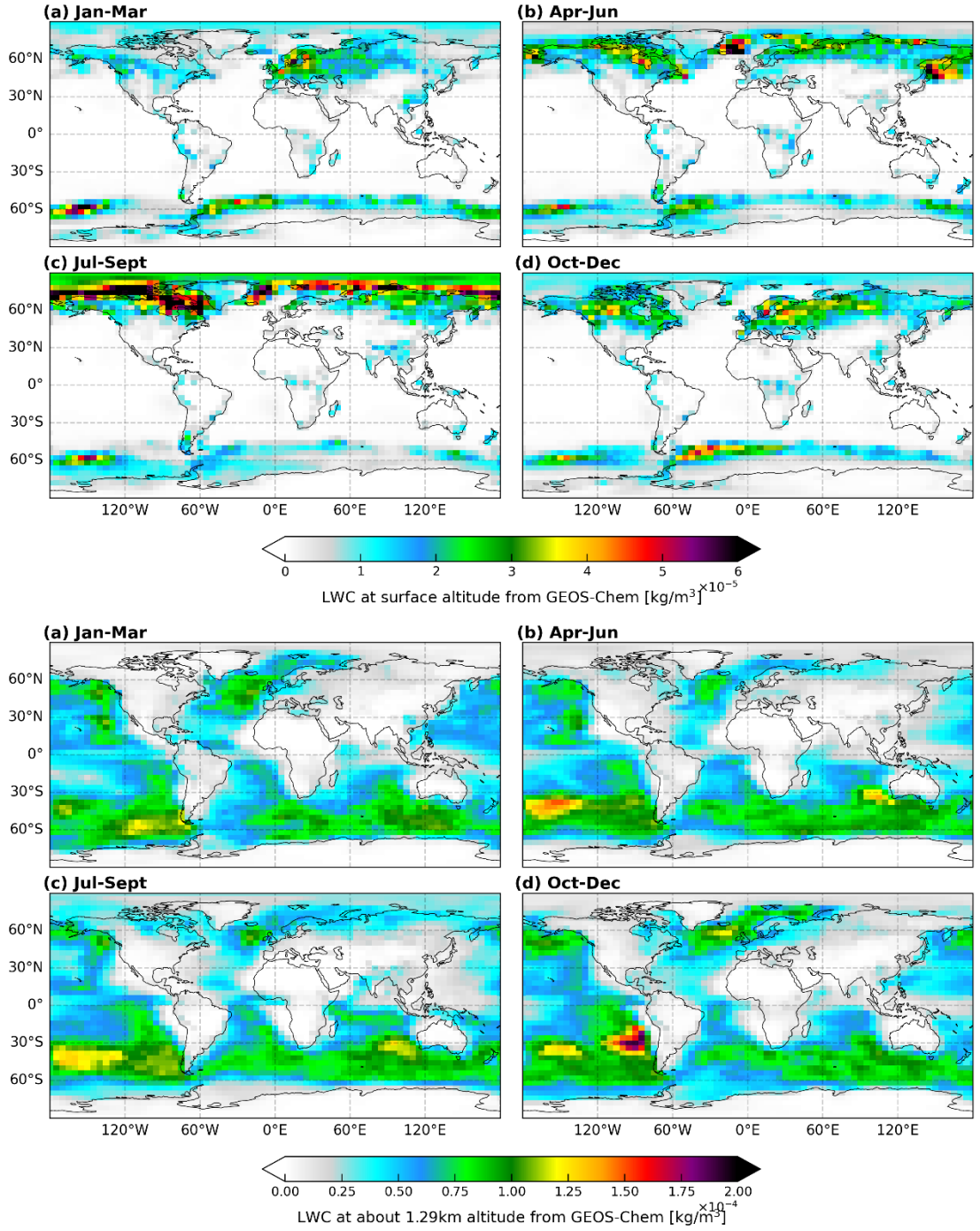

Fig. S27. The liquid water content in 2023 for different seasons at surface and 1.29 km altitude.

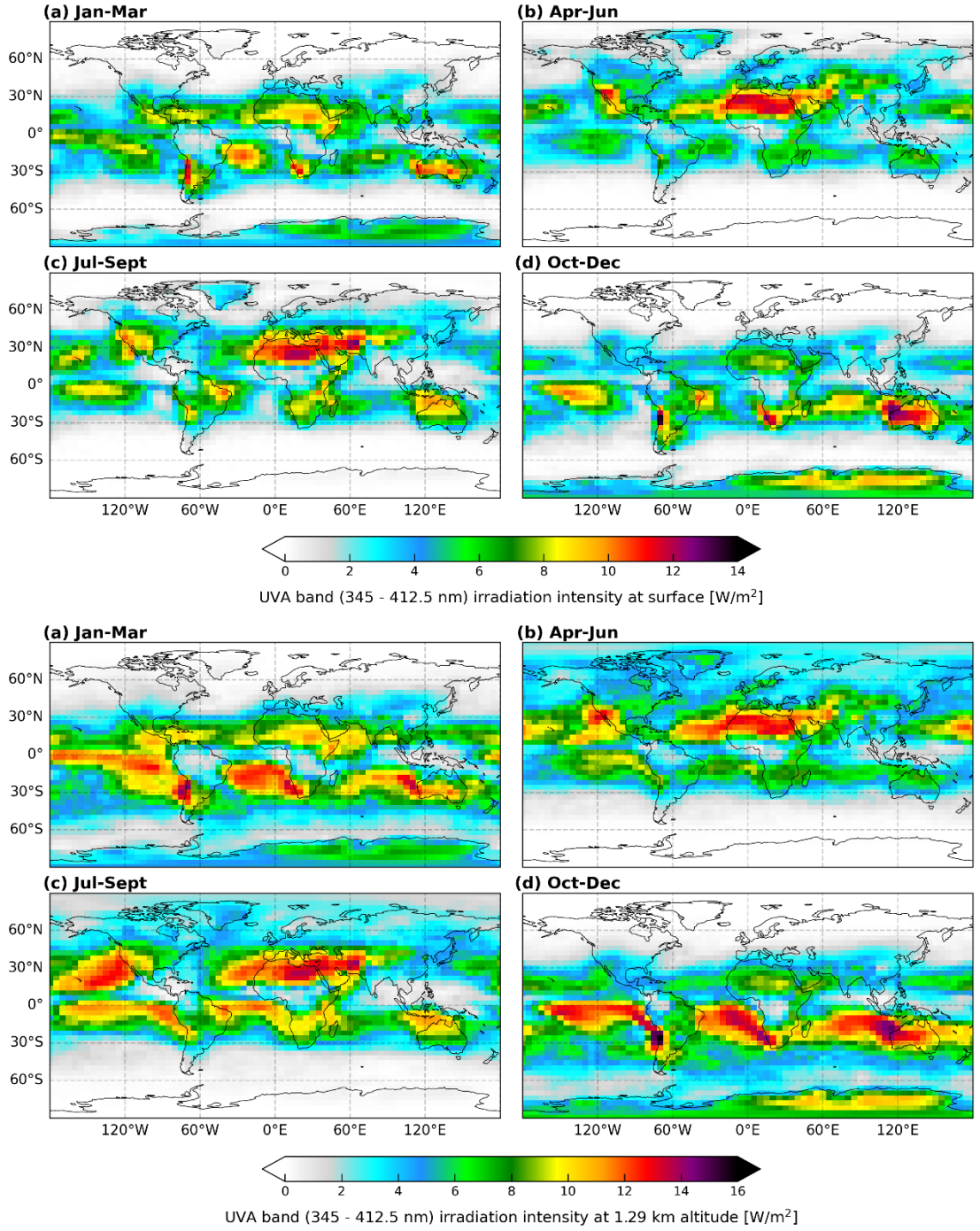

Fig. S28. The global UVA direct irradiation intensity in 2023 for different seasons at surface and 1.29 km altitude.

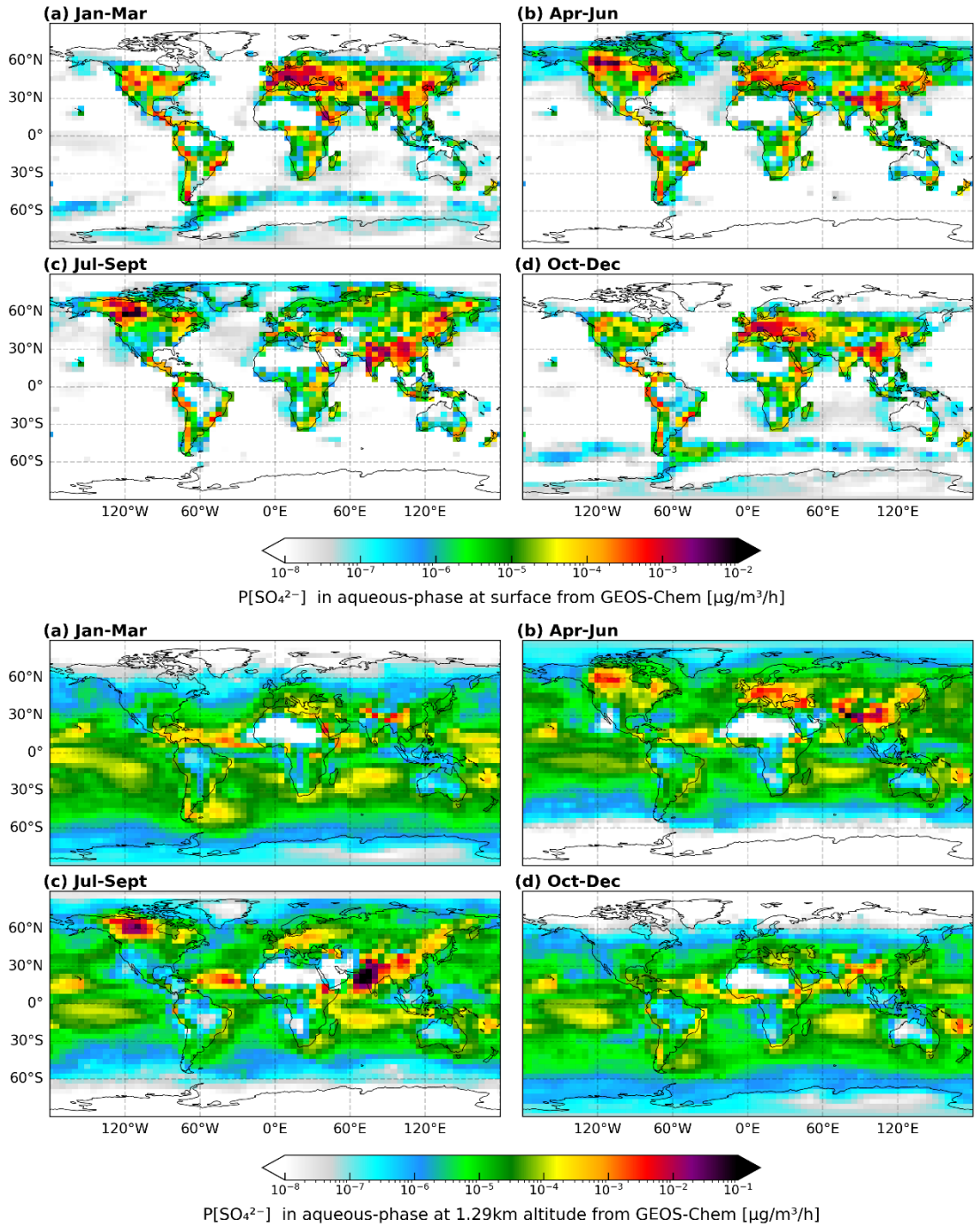

Fig. S29. The rate of SO_4^{2-} formation from the photolysis of S(IV) in aqueous phase in 2023 for different seasons at surface and 1.29 km altitude.

Table S1. The S(IV) oxidation reaction with H_2O_2 and its rate constant [2].

Reaction	k (M^{-1} s^{-1})
$O_2^{\bullet-} + H^+ \rightarrow HO_2\bullet$	3.56×10^{10}
$HO_2\bullet + HO_2\bullet \rightarrow H_2O_2 + O_2$	8.6×10^5
$S(IV) + O_2^{\bullet-} + H2O \rightarrow S(VI) + OH\bullet + OH^-$	1.0×10^5
$S(IV) + HO_2\bullet \rightarrow S(VI) + OH\bullet$	1.0×10^6
$S(IV) + OH\bullet \rightarrow S(VI) + OH\bullet$	4.5×10^9
$S(IV) + H_2O_2 \rightarrow S(VI) + H_2O$	7.5×10^7

References

1 McFall, A. S., Johnson, A. W. & Anastasio, C. Air–Water Partitioning of Biomass-Burning Phenols and the Effects of Temperature and Salinity. *Environ. Sci. Technol.* **54**, 3823–3830 (2020).

2 John H. Seinfeld & Pandis, S. N. *ATMOSPHERIC CHEMISTRY AND PHYSICS From Air Pollution to Climate Change Third Edition*. (Wiley, 2016).

3 Tran, L. N., Abellar, K. A., Cope, J. D. & Nguyen, T. B. Second-Order Kinetic Rate Coefficients for the Aqueous-Phase Sulfate Radical ($SO_4^{\bullet-}$) Oxidation of Some Atmospherically Relevant Organic Compounds. *J. Phys. Chem. A* **126**, 6517–6525 (2022).